

**NIST Interagency Report  
NIST IR 8488**

# **Repeatability of Contactless and Contact Fingerprint Capture**

John Libert  
Shahram Orandi  
John Grantham  
Kenneth Ko  
Bruce Bandini

This publication is available free of charge from:  
<https://doi.org/10.6028/NIST.IR.8488>

**NIST Interagency Report  
NIST IR 8488**

# **Repeatability of Contactless and Contact Fingerprint Capture**

John Libert  
Shahram Orandi  
Kenneth Ko  
Bruce Bandini  
*Image Group  
Information Access Division  
Information Technology Laboratory*

John Grantham  
*Systems Plus, Inc.  
Rockville, MD*

This publication is available free of charge from:  
<https://doi.org/10.6028/NIST.IR.8488>

September 2023



U.S. Department of Commerce  
*Gina M. Raimondo, Secretary*

National Institute of Standards and Technology  
*Laurie E. Locascio, NIST Director and Under Secretary of Commerce for Standards and Technology*

NIST IR 8488  
September 2023

Certain commercial equipment, instruments, software, or materials, commercial or non-commercial, are identified in this paper in order to specify the experimental procedure adequately. Such identification does not imply recommendation or endorsement of any product or service by NIST, nor does it imply that the materials or equipment identified are necessarily the best available for the purpose.

Covered by NIST Research Protection Office (RPO) protocol CTL-2021-0300.

### **NIST Technical Series Policies**

[Copyright, Use, and Licensing Statements](#)

[NIST Technical Series Publication Identifier Syntax](#)

### **Publication History**

Approved by the NIST Editorial Review Board on 2023-09-12

### **How to Cite this NIST Technical Series Publication**

Libert J, Orandi S, Grantham J, Ko K, Bandini B (2023) Repeatability of Contactless and Contact Fingerprint Capture. (National Institute of Standards and Technology, Gaithersburg, MD), NIST Interagency Report (IR) NIST IR 8488. <https://doi.org/10.6028/NIST.IR.8488>

### **NIST Author ORCID iDs**

John Libert: 0000-0003-0796-6871

Shahram Orandi: 0000-0002-5390-6119

John Grantham: 0000-0003-2219-0944

Kenneth Ko: 0000-0002-6409-1592

Bruce Bandini: 0000-0003-0608-6426

### **Contact Information**

[fastcap@nist.gov](mailto:fastcap@nist.gov)

## **Abstract**

A new generation of contactless fingerprint capture devices has recently emerged. These devices provide the ability to capture a fingerprint without making physical contact with the finger. There is anecdotal evidence that the process of capturing a fingerprint when physical contact is made introduces a certain amount of physical distortion to the finger being pressed against the collection medium. It is hypothesized that because contactless collection devices do not need to make physical contact with the finger being captured, the resulting collections from contactless devices are expected to have no mechanical deformation introduced to the finger and provide better intraoperability than contact devices and better consistency between captures from the same device.

This hypothesis was rejected in that observations in this study showed that contact collection devices have more consistency and less variability between successive captures using the same device. Thus, while contactless devices carry with them the promise of faster capture without making any contact with the subject, the images captured by these devices may have greater variability across successive captures and accordingly impact on performance relative to that of contact-collected images should be tested further.

## **Keywords**

Contactless fingerprint; fingerprint; minutiae displacement; SIVV; skin distortion; Spectral Validation Verification Metric; Structural Similarity Index Metric; SSIM.

## Table of Contents

<b>1. Introduction</b> .....	<b>1</b>
<b>2. Method</b> .....	<b>2</b>
2.1. Data .....	2
2.2. NFRaCT Comparison.....	3
2.3. Analysis .....	4
2.3.1. Free Minutia Pair Displacement .....	4
2.3.2. Mean Minutiae Displacement .....	4
2.3.3. Scale Factor.....	5
2.3.4. Comparison Score.....	5
2.3.5. Structural Similarity Index (SSIM) .....	5
2.3.6. Ridge Orientation Correlation.....	6
2.3.7. Inverse RMS Difference of Spectral Image Validation Verification (SIVV) Signals ....	7
2.3.8. SIVV Correlation.....	7
<b>3. Results and Discussion</b> .....	<b>8</b>
3.1. Free Minutiae Pair Displacement.....	8
3.2. Mean Minutiae Pair Displacement.....	9
3.3. Scale Factor .....	10
3.4. Comparison Score.....	11
3.5. Structural Similarity Index (SSIM).....	12
3.6. Ridge Orientation Correlation .....	14
3.7. Inverse RMS Difference of Spectral Image Validation Verification (SIVV) Signals .....	14
3.8. SIVV Correlation.....	15
<b>4. Conclusions</b> .....	<b>16</b>
<b>References</b> .....	<b>18</b>
<b>Appendix A. Glossary</b> .....	<b>21</b>
<b>Appendix B. Box and Whisker Plots</b> .....	<b>22</b>

## List of Tables

Table 1 – Image pairs successfully registered .....	4
---	---

## List of Figures

Figure 1 – Distributions of displacement of the “free minutiae pair” for contact devices 02, 03, and 04 compared to that of mobile contactless fingerprint capture devices. ....	8
--	---

Figure 2 – Distributions of mean displacement of all minutiae pairs detected by the SourceAFIS comparison algorithm for contact devices 02, 03, and 04 compared to that of mobile contactless fingerprint capture devices..... 9

Figure 3 – Distributions of Scale Factor measurements computed from the offset distance of the reference “fixed” minutia of the registered images to the “free” minutia..... 10

Figure 4 – Distributions of mated comparison scores for contact devices 02, 03, and 04 compared to that of mobile contactless fingerprint capture devices..... 11

Figure 5 – Distributions of Structural Similarity Index (SSIM) for contact devices 02, 03, and 04 compared to that of mobile contactless fingerprint capture devices..... 13

Figure 6 – Distributions of Ridge Orientation Correlation for contact devices 02, 03, and 04 compared to that of mobile contactless fingerprint capture devices..... 14

Figure 7 – Distributions of inverse RMSD off SIVV signals for contact devices 02, 03, and 04 compared to that of mobile contactless fingerprint capture devices..... 15

Figure 8 – Distributions of Correlation of SIVV signals for contact devices 02, 03, and 04 compared to that of mobile contactless fingerprint capture devices..... 16

Figure 9 – Relationship between the boxplot of normally distributed data compared to the standard normal distribution for illustrative purposes. [36] ..... 22

## **Acknowledgments**

Special thanks are due to our colleagues, John Belz, Gary Horwarth, and the mFIT<sup>1</sup> team of the Public Safety Communications Research Division of NIST in Boulder, Colorado who collected the images used in the present study and to the NIST Federal Employee volunteers in Boulder who during Coronavirus restrictions contributed their fingerprints to the mFIT competition and to additional NIST examination.

---

<sup>1</sup> mFIT refers to the Mobile Fingerprinting Innovation Technology challenge sponsored by the Public Safety Communications Research (PSCR) Division of the National Institute of Standards and Technology (NIST) of Boulder, CO with technical consultation in fingerprint biometrics supplied by the Image Group of the NIST Information Access Division of the Information Technology Laboratory of Gaithersburg, MD.

## 1. Introduction

Significant research has been conducted to examine interoperability of contactless fingerprint devices with legacy contact collection devices [1][14][15][16][12]. However, little has been offered regarding intraoperability, or repeatability and consistency in captures for the same device. Examining intraoperability can uncover causes of pattern variation present for a sensor. In this study, our focus was not interoperability of contactless with contact collection fingerprint capture devices; rather we examine consistency of a repeated pattern acquisition with the same device. Such would have direct bearing, for example, on the use of such devices for personal identity verification (PIV) where the same device may be used to make successive collections for verification of identity within a short period of time. While conducting this research, we attempt to quantify the consistency of capture through the selection of a set of fidelity metrics that were identified in [28].

Of particular interest here is the comparative displacement of corresponding minutiae in repeat/successive fingerprint captures. It has long been known that with contact capture of fingerprints, deformation, or distortion of the skin due to pressure, may result in nonlinear displacements of features used for comparison in an Automated Fingerprint Identification System (AFIS) [2][3][4][5][6]. It has been suggested that contactless collection does not introduce any deformation distortion since no pressure is applied to the skin [7][10][11].

Contact collection requires applying mechanical pressure by the finger to a collection medium and given the natural plasticity of a finger, this mechanical pressure can introduce deformation to the finger relative to its original shape.

It was hypothesized that because contactless collection devices do not require any mechanical force on the finger to conduct a collection, the deformation normally introduced to fingers during contact collection would not be present in contactless collection.

Furthermore, repeated fingerprint collection in close temporal adjacency on the order of seconds will yield fingerprint images that have had minimal environmental impact introduced because of delayed capture. Therefore, it was hypothesized that because contactless collection devices do not introduce any mechanical deformation to the finger, the resulting collections made in close temporal proximity from the same contactless devices are expected to have better intraoperability and more consistency between captures.

A few investigators have attempted to develop methods by which to correct fingerprints for such deformation to improve performance in an AFIS [7][10][11][20][21][22]. As observed recently by several researchers, contactless capture avoids skin distortion [7][10][11]. While not directly claimed, the implication is that minutiae or singular features used for matching avoid the displacement that might occur with skin deformation typical of contact acquisition of fingerprints. While true that contactless fingerprint capture avoids mechanically induced minutiae displacement due to skin deformation, we are interested here in testing whether this yields measurably smaller displacement of corresponding minutiae across a pair of fingerprints sampled with contactless devices relative to that for contact devices.

## 2. Method

### 2.1. Data

Fingerprint images were collected from 99 Federal Employee volunteers at the National Institute of Standards and Technology (NIST) facility in Boulder, CO in support of the Mobile Fingerprinting Innovation Technology (mFIT) Challenge [1]. Fingerprints were acquired using three Appendix F [25] FBI certified devices and six mobile fingerprint capture applications installed on smartphone devices. Two samples of index and middle fingers from each hand were acquired in close succession of time from each subject using each of the devices. This yielded 396 pairs of fingerprint images for comparison from each of the devices. Contact (Appendix F) devices yielded fingerprint images at 500 pixels per inch (ppi)<sup>2</sup> or 19.7 pixels per millimeter (ppmm) and contactless devices yielded images targeted<sup>3</sup> at 500 ppi.

---

<sup>2</sup> Resolution values for fingerprint imagery are specified in pixels per inch (ppi) throughout this document. This is based on widely used specification guidelines for such imagery and is accepted as common nomenclature within the industry. SI units for these will be presented only once.

<sup>3</sup> Contactless devices are calibrated to produce images of 500 ppi, though for these devices the sample rate is imprecise relative to that of contact fingerprint acquisition.

## 2.2. NFRaCT Comparison

To facilitate this study, fingerprint image pairs were compared using NFRaCT. As described in [28], NFRaCT performs rigid registration [31] of the image pair using sets of corresponding minutiae points. These sets of corresponding minutiae points can be either automatically detected by the software or interactively selected by the operator. Rigid registration of image pairs facilitates our analysis while preserving any deformation that may have been introduced between subsequent captures. Hence, given a pair of corresponding images,  $I_1$  and  $I_2$ , registration and cropping to areas of overlap, yields images,  $I'_1$  and  $I'_2$ , used for all measurements requiring images of equal dimension and region correspondence.

For most image pairs, NFRaCT's utilization of the open-source comparison algorithm, SourceAFIS [30] was able to automatically detect up to five pairs of corresponding minutiae. For image pairs where this automatic operation failed, the operator attempted to select at least two pairs of corresponding minutiae or other landmarks<sup>4</sup> to support rigid registration of the fingerprint pairs. When this manual selection of registration points was not possible processing could not proceed resulting in loss of data for the purpose of this study. The sample sizes were adjusted accordingly due to inability to register the image pair.

Given the 99 subjects, each contributing four fingers for each of two captures, the expected total number of finger pairs (encounter 1 and encounter 2) for each device should have been 396. While examining the data via the NIST Fingerprint Registration and Comparison Tool (NFRaCT) [28], we noticed several cases of fingerprint mislabeling preventing registration and consequent data loss. In other cases, one of the paired fingerprints had some image quality issues of sufficient impact as to prevent SourceAFIS from identifying at least two pairs of corresponding minutiae points needed for the rigid registration of fingerprint images. If it was not possible for these image pairs to be recovered via manual selection of minutiae points, these cases would also be missing from the analysis. Thus, the sample sizes repeated in all the preceding plots may represent roughly the general quality of images collected by each of the devices. They are not failures to acquire, per se, as images were acquired. The image quality of one or both images in these cases prevented comparison that relied upon registration [31].

---

<sup>4</sup> In some fingers, the friction ridge pattern might be damaged such that features such as cracks or fissures can be used as control points instead of ridge bifurcations or endings normally identified as "minutiae."

Table 1 – Image pairs successfully registered

<b>Device</b>	<b>Samples</b>
<b>02</b>	388
<b>03</b>	386
<b>04</b>	380
<b>05</b>	206
<b>06</b>	351
<b>09</b>	338
<b>10</b>	330
<b>12</b>	317
<b>13</b>	384

## **2.3. Analysis**

NFRaCT outputs results of the image comparisons it performs as an Extensible Markup Language (XML) file containing the measurands detailed in [28]. A subset of the data contained in the XML file is then extracted and collated for the present analysis. The measurands used for this study are described in this section.

### **2.3.1. Free Minutia Pair Displacement**

In NFRaCT, registration of a pair of images is performed as a two-step process: First, the moving image is translated such that one set of control points is brought into coincidence with those of the fixed image. This pair of points is referred to as ‘constrained,’ as the distance between these two points will always be zero. Then, the moving image is rotated such that the other pair of points are brought into closest proximity. This pair of points is referred to as ‘unconstrained’ or ‘free’ and the Euclidean distance of their offset is taken as this metric. When multiple registration attempts occur due to the selection of more than two pairs of registration candidate points, this metric will represent the offset between the free pair of points that yielded the registration transform which maximized the Mean Structural Similarity Index Metric (MSSIM) [32]**Error! Reference source not found.** value (i.e., the optimal registration result for a set of registration candidates).

### **2.3.2. Mean Minutiae Displacement**

As mentioned previously, each combination of corresponding minutiae is used to perform a candidate transformation. The displacement of minutiae pairs in each case is tabulated and the mean reported as one of our metrics. The NFRaCT GUI displays up to five pairs of corresponding minutiae, but the SourceAFIS algorithm finds more than this. The selection of the optimum transform considers all pairs as does the calculation of mean minutiae displacement, the value of which can be influenced by the number of minutiae pairs available for this computation.

### 2.3.3. Scale Factor

Given that the points selected from the image pair correspond, we compute a scale factor by comparing the distances between the point pairs on the two images. Hence, given that we have two images  $I_1$  and  $I_2$ , we can designate sampled points from  $I_1$  as  $P_{1x_1}$ ,  $P_{1y_1}$ , and  $P_{1x_2}$ ,  $P_{1y_2}$ . Corresponding points sampled from  $I_2$  are then  $P_{2x_1}$ ,  $P_{2y_1}$ , and  $P_{2x_2}$ ,  $P_{2y_2}$ . We calculate the distances between the sampled points as

$$\begin{aligned}d_1 &= \sqrt{(P_{1x_2} - P_{1x_1})^2 + (P_{1y_2} - P_{1y_1})^2} \\d_2 &= \sqrt{(P_{2x_2} - P_{2x_1})^2 + (P_{2y_2} - P_{2y_1})^2}\end{aligned}\tag{1}$$

The scale factor is the ratio between the two distances

$$SF = \frac{\min(d_1, d_2)}{\max(d_1, d_2)}\tag{2}$$

### 2.3.4. Comparison Score

The Comparison Score is the comparison score yielded by SourceAFIS **Error! Reference source not found.**

### 2.3.5. Structural Similarity Index (SSIM)

The Structural Similarity Index (SSIM) [32] compares a pair of registered images, assessing their visual similarity. The formulation is applied block-wise to corresponding Regions of Interest (ROIs) of the registered images,  $I'_1$  and  $I'_2$ , and then pooled via averaging over all blocks to yield a single figure of merit for similarity of the image pair. Moving an 11 x 11 block over each pixel of the image with padding on the edges yields a matrix of structural similarity values equal in dimension to the images under comparison.

The SSIM quality assessment is based on the computation of three terms, namely the luminance term, the contrast term, and the structural term. The overall index is a multiplicative combination of the three terms.

$$SSIM(x, y) = [l(x, y)]^\alpha [c(x, y)]^\beta [s(x, y)]^\gamma$$

where

$$l(x, y) = \frac{2\mu_x\mu_y + C_1}{\mu_x^2 + \mu_y^2 + C_1},$$

$$c(x, y) = \frac{2\sigma_x\sigma_y + C_2}{\sigma_x^2 + \sigma_y^2 + C_2},$$

$$s(x, y) = \frac{\sigma_{xy} + C_3}{\sigma_x\sigma_y + C_3},$$

(3)

Where  $\mu_x, \mu_y, \sigma_x, \sigma_y,$  and  $\sigma_{xy}$  are local means, standard deviations, and cross-covariance for images  $x, y$ .

By default, regularization constants for the three components, luminance, contrast, and structure are

- $C_1 = (0.01 * L)^2$ , where  $L$  is the specified dynamic range value of 255.
- $C_2 = (0.03 * L)^2$ , where  $L$  is the specified dynamic range value of 255.
- $C_3 = C_2/2$ .

The SSIM function uses these regularization constants to avoid instability for image regions where the local mean or standard deviation is close to zero. Therefore, small non-zero values should be used for these constants.

We set  $\alpha = \beta = \gamma = 1.0$ . This simplifies the formula to

$$SSIM(x, y) = \frac{(2\mu_x\mu_y + C_1)(2\sigma_{xy} + C_2)}{(\mu_x^2 + \mu_y^2 + C_1)(\sigma_x^2 + \sigma_y^2 + C_3)} \quad (4)$$

The SSIM values are pooled by averaging, hence we have the Mean SSIM, or MSSIM.

### 2.3.6. Ridge Orientation Correlation

We compare via correlation the block-wise estimates of ridge orientation. We create an orientation map of ridge orientation for each of the two overlapping regions of the registered images,  $I_1$  and  $I_2$ . For this we apply the method described in [33] as modified by Kovessi for a MATLAB function [34]. The method estimates the local orientation of ridges within a 7 x 7-pixel block centered on each pixel of the image being processed. The output is a map of angles in radians corresponding to the size of the input image. Thus, applying the procedure to the cropped

regions of overlap,  $I'_1$  and  $I'_2$ , we get orientation maps,  $O_1$  and  $O_2$ . We then compute the 2D correlation of the two orientation maps.

### 2.3.7. Inverse RMS Difference of Spectral Image Validation Verification (SIVV) Signals

Both differences and ratios of SIVV signals can provide quantitative measures for the comparison of images. For the present study, we examine image differences between pairs of images,  $I'_1$  and  $I'_2$ , with respect to the Root Mean Squared Difference (RMSD) between their two SIVV signals,  $s_1$  and  $s_2$ , over the entire frequency range 0 - 0.5 cycles/pixel.

$$1 - RMSD(s_1, s_2) = \sqrt{\frac{\sum_{i=1}^n (s_{1,i} - s_{2,i})^2}{n}} \quad (5)$$

where  $n = |s_1| = |s_2|$  (i.e., the lengths of the signal vectors).

We subtract the RMSD from one such that higher inverted RMSD scores will correspond with greater spectral similarity between the two images.

### 2.3.8. SIVV Correlation

The RMSD measures the total deviation of point-wise comparison of the SIVV signals. The Pearson product moment correlation coefficient measures the parallelism between the two signals irrespective of the magnitude of the difference between them. Accordingly, we compute the correlation coefficient between  $s_1$  and  $s_2$  as

$$r(s_1, s_2) = \frac{\sum_{i=1}^n (s_1 - \bar{s}_1)(s_2 - \bar{s}_2)}{\sqrt{\sum_{i=1}^n (s_1 - \bar{s}_1)^2} \sqrt{\sum_{i=1}^n (s_2 - \bar{s}_2)^2}} \quad (6)$$

where  $\bar{s}_1$  and  $\bar{s}_2$  are the arithmetic means of their respective SIVV signal vectors.

### 3. Results and Discussion

#### 3.1. Free Minutiae Pair Displacement

Despite possible minutiae displacement due to skin deformation in contact fingerprint capture, we see from our direct measurements of corresponding minutiae displacement that contact devices have lower median displacement and smaller variation than contactless devices. Thus, while true that contactless capture avoids potential problems of skin deformation, this displacement appears more consistent (and smaller) within captures from contact devices and collection from contact devices shows less variation with respect to minutiae displacement.

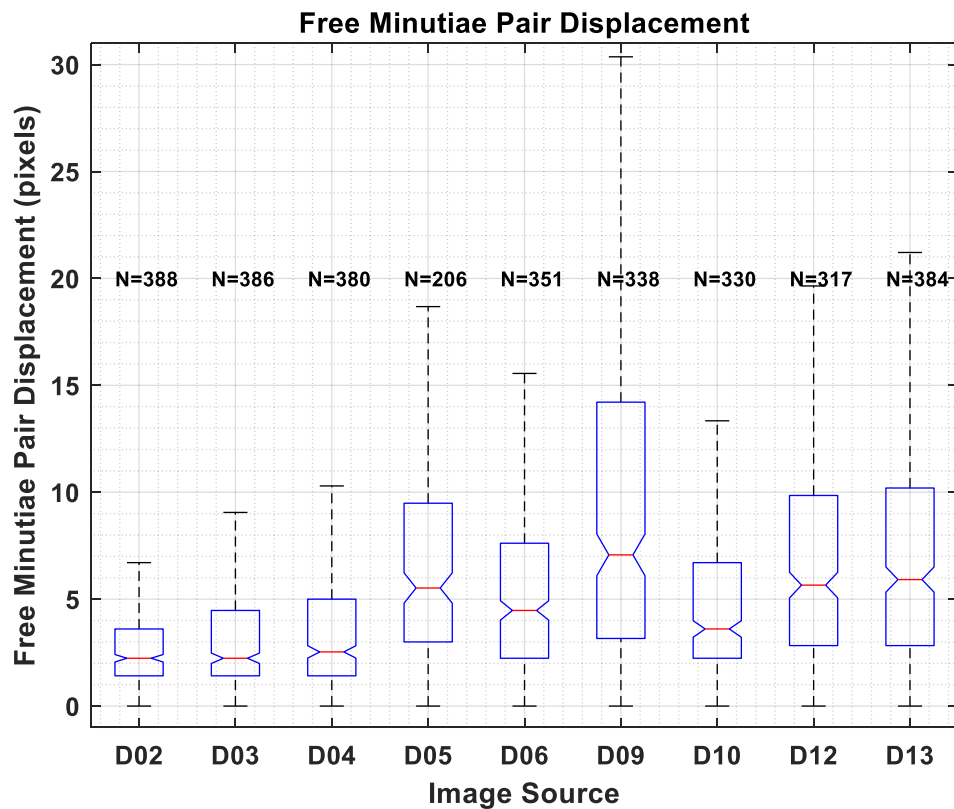


Figure 1 – Distributions of displacement of the “free minutiae pair” for contact devices 02, 03, and 04 compared to that of mobile contactless fingerprint capture devices.

Small displacement is clearly the case with contact capture of “plain” or “flat” fingerprint impressions. It is possible that this aspect of repeatability may be impacted to a greater extent with acquisition of rolled fingerprints – to be studied in subsequent experiments. However, the mobile contactless devices such as those used in the mFIT Challenge can capture more friction ridge area than that captured in a slap-four contact acquisition. With contactless collection, much

Legend:	D02 : Contact, Electroluminescent	D03 : Contact, FTIR	D04 : Contact, FTIR	D05 : Contactless, Mobile	D06 : Contactless, Mobile
	D07 : Contactless, Mobile	D09 : Contactless, Mobile	D10 : Contactless, Mobile	D12 : Contactless, Mobile	D13 : Contactless, Mobile

of the additional area of friction ridge is generally less useful due to imaging problems such as poor focus, poor lighting (shadow and specularities), and parallax deformation. Even in areas of good focus, lighting polarity inversion [13] has been observed and may account for some apparent minutiae displacement. For example, with polarity inversion a minutiae may change from bifurcation to ridge ending thereby resulting in a small shift in location with respect to the same image that is not impacted by this inversion. SourceAFIS **Error! Reference source not found.** does consider minutiae type in establishing the score for a fingerprint comparison but does not require minutiae to be of the same type in establishing correspondence.

### 3.2. Mean Minutiae Pair Displacement

As described in [28], NFRaCT measures the distance between all corresponding minutiae pairs detected by the SourceAFIS module and reports the mean of these measurements. Displacement for all corresponding minutiae pairs identified by the SourceAFIS matcher shows higher medians for all contactless devices. This displacement is on average five or fewer pixels offset for contact devices, and up to twice that many for contactless devices with greater variability in displacement distance.

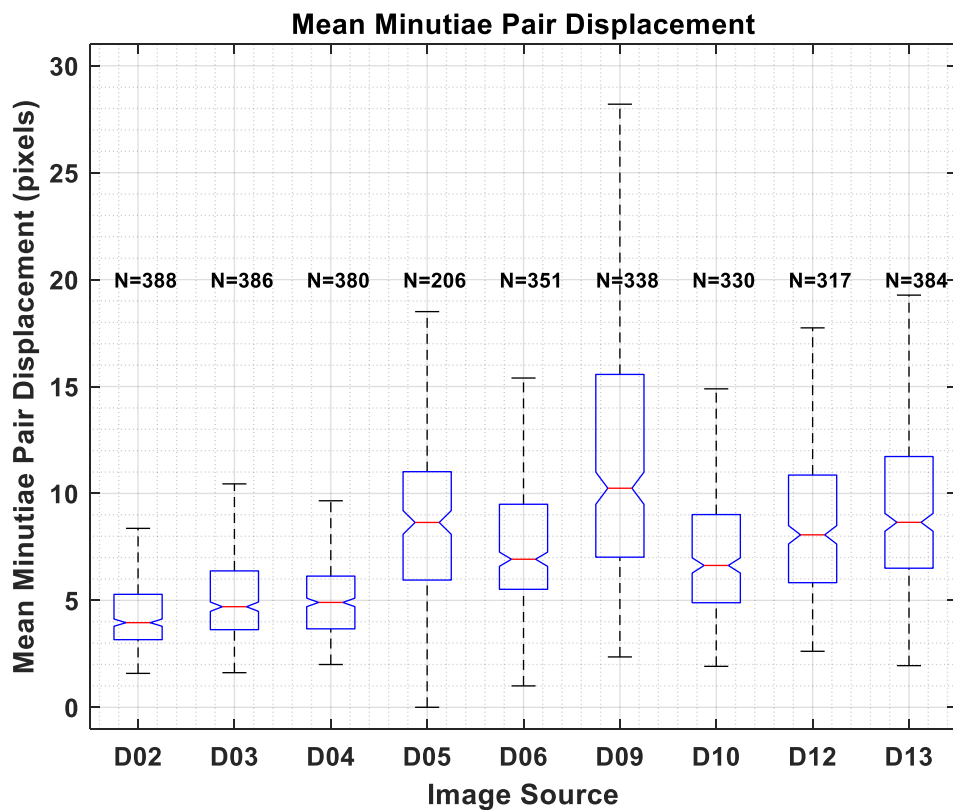


Figure 2 – Distributions of mean displacement of all minutiae pairs detected by the SourceAFIS comparison algorithm for contact devices 02, 03, and 04 compared to that of mobile contactless fingerprint capture devices.

Legend:	D02 : Contact, Electroluminescent	D03 : Contact, FTIR	D04 : Contact, FTIR	D05 : Contactless, Mobile	D06 : Contactless, Mobile
	D07 : Contactless, Mobile	D09 : Contactless, Mobile	D10 : Contactless, Mobile	D12 : Contactless, Mobile	D13 : Contactless, Mobile

### 3.3. Scale Factor

Based on anecdotal observations in prior data collections, scale control remains a challenge for contactless fingerprint capture due to the relatively unconstrained capture geometries of the mobile devices. Scale, of course, has a direct impact on image sample rate which in turn must conform to expectations on fingerprint comparison systems. The FBI EBTS Appendix F [25] specifies that fingerprint images must be sampled at 500 pixels per inch (ppi) with a tolerance of one percent, or  $\pm 5$  ppi. The less demanding specification for Personal Identity Verification (PIV) devices [26] allows a tolerance of two percent, or  $\pm 10$  ppi for an expected 500 ppi sample rate.

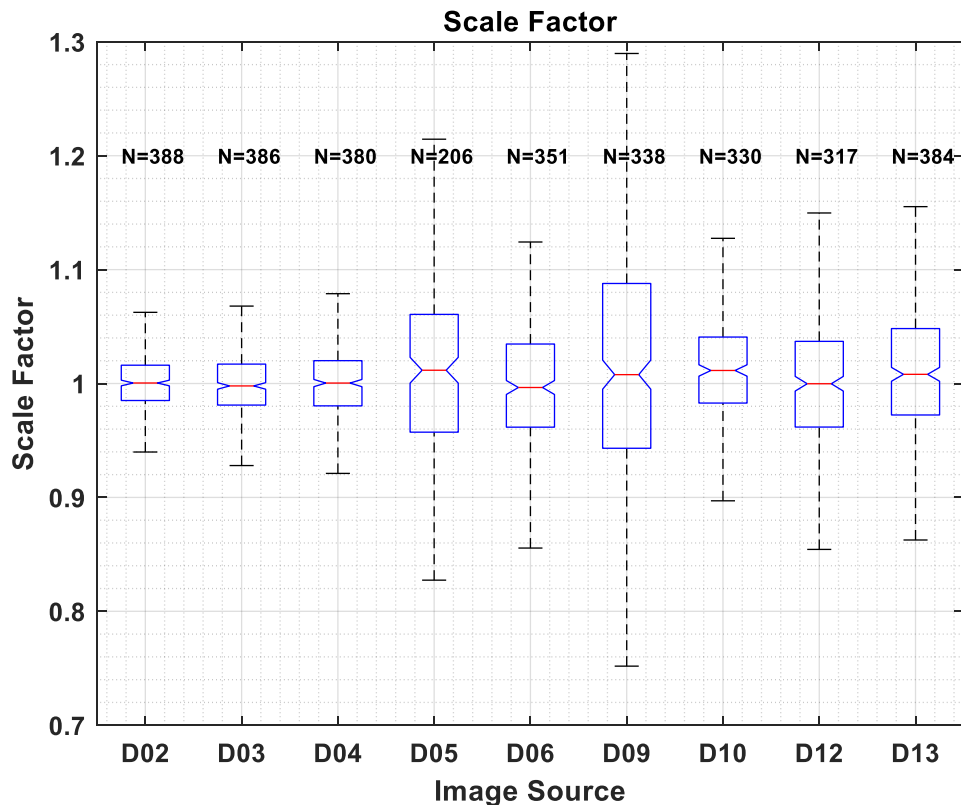


Figure 3 – Distributions of Scale Factor measurements computed from the offset distance of the reference “fixed” minutia of the registered images to the “free” minutia.

We see very consistent image capture scale for repeat contact collected fingerprints, with the median of 1.0 at the desired sample rate. In Figure 3 we see that the boxes and at least half of the “whiskers” for the contact devices are fully within one percent shows these devices to be largely conformant to the Appendix F standard. This is not surprising as the capture geometry of the contact devices would be relatively constant with only pressure variation on the platen accounting for the observed variability.

Legend:	D02 : Contact, Electroluminescent	D03 : Contact, FTIR	D04 : Contact, FTIR	D05 : Contactless, Mobile	D06 : Contactless, Mobile
	D07 : Contactless, Mobile	D09 : Contactless, Mobile	D10 : Contactless, Mobile	D12 : Contactless, Mobile	D13 : Contactless, Mobile

Only two of the mobile contactless devices, D06 and D12, show medians of 1.0 but with higher variability than that of the contact devices. Other contactless devices show both higher median values and greater variability. The geometry of contactless capture is not as well constrained relative to contact acquisition, but these devices show reasonable control of scale relative to that observed in earlier measurements [13][14], and most of their distributions fall within the PIV “two percent” specification.

### 3.4. Comparison Score

In nearly all cases, the contactless devices yielded lower comparison similarity scores between repeat captures compared to contact-collected images being matched to other contact-collected images from the same device. We find it notable that one of the contactless devices, D13, a smartphone based contactless collection device, reaches scores comparable to contact collection devices and was the exception in the aforementioned observation. That being said, scores from D13 do still show higher variability when compared to a contact collection device.

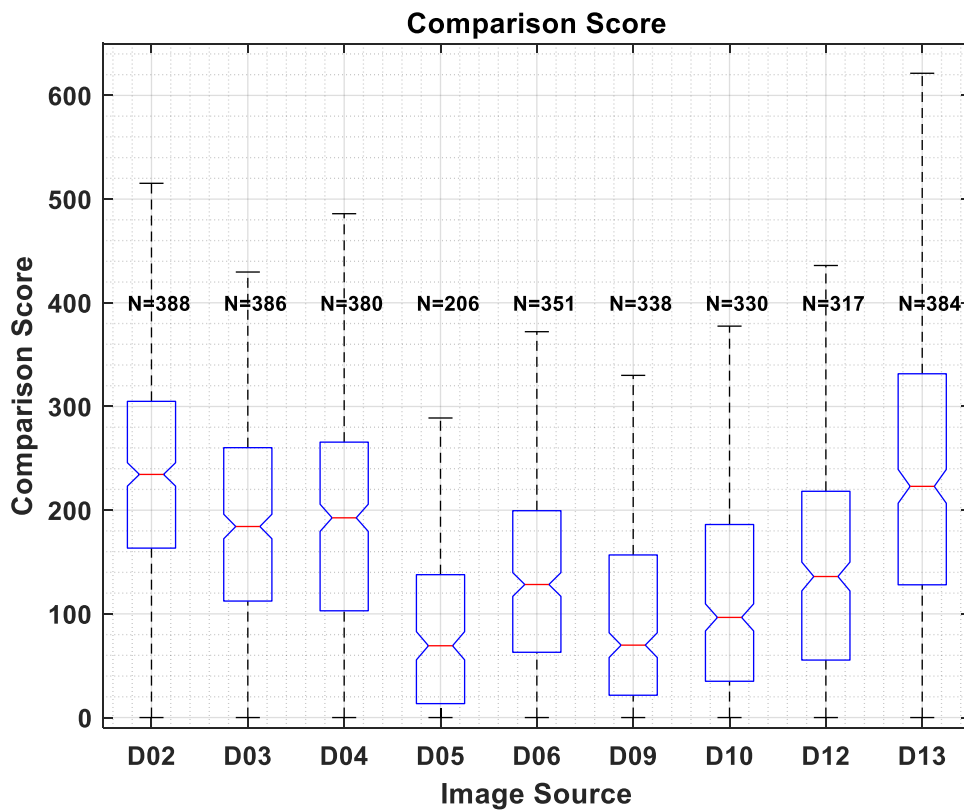


Figure 4 – Distributions of mated comparison scores for contact devices 02, 03, and 04 compared to that of mobile contactless fingerprint capture devices.

Legend:	D02 : Contact, Electroluminescent	D03 : Contact, FTIR	D04 : Contact, FTIR	D05 : Contactless, Mobile	D06 : Contactless, Mobile
	D07 : Contactless, Mobile	D09 : Contactless, Mobile	D10 : Contactless, Mobile	D12 : Contactless, Mobile	D13 : Contactless, Mobile

Keep in mind that these comparison scores are for pairs of images collected from identical fingers sampled closely in time using the same device. Anecdotally, a very high comparison score is expected in this well constrained one-to-one scenario with close longitudinal adjacency.

### 3.5. Structural Similarity Index (SSIM)

The Structural Similarity Index Metric measures on a block-wise basis the fidelity between a pair of registered images based on local similarity of luminance (gray level), contrast, and structure. With a maximum value of 1.0 for identical images we see in Figure 5 that even the contact images are far from identical. The three contact collection devices do however show higher SSIM (i.e., greater structural similarity) between successive captures than do the contactless devices.

What is interesting is the disproportionately higher SSIM for D02 relative to D03 and D04. D02 uses electro-luminescent technology in contrast to the FTIR optical technology of the other two contact devices. While this finding may be a function of the small subject pool, it is pronounced enough to warrant further investigation in future studies.

Legend:	D02 : Contact, Electroluminescent	D03 : Contact, FTIR	D04 : Contact, FTIR	D05 : Contactless, Mobile	D06 : Contactless, Mobile
	D07 : Contactless, Mobile	D09 : Contactless, Mobile	D10 : Contactless, Mobile	D12 : Contactless, Mobile	D13 : Contactless, Mobile

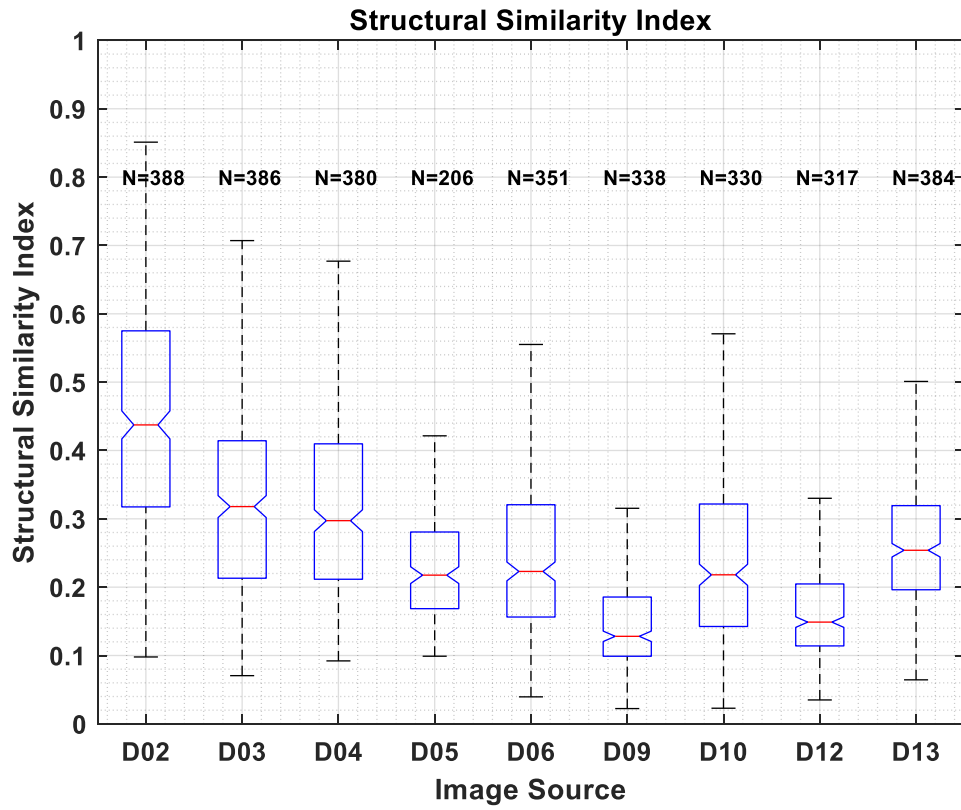


Figure 5 – Distributions of Structural Similarity Index (SSIM) for contact devices 02, 03, and 04 compared to that of mobile contactless fingerprint capture devices

Legend:	D02 : Contact, Electroluminescent	D03 : Contact, FTIR	D04 : Contact, FTIR	D05 : Contactless, Mobile	D06 : Contactless, Mobile
	D07 : Contactless, Mobile	D09 : Contactless, Mobile	D10 : Contactless, Mobile	D12 : Contactless, Mobile	D13 : Contactless, Mobile

### 3.6. Ridge Orientation Correlation

Figure 6 shows higher correlations of local ridge orientation for contact images in contrast to contactless. Ridge orientation represents the angle orthogonal to the dominant gradient in a  $7 \times 7$  block sample of the image. This calculation can be adversely affected by feature noise [13] where a spurious feature is created by the rendering algorithm where the actual ridge is not apparent possibly due to poor focus or lighting.

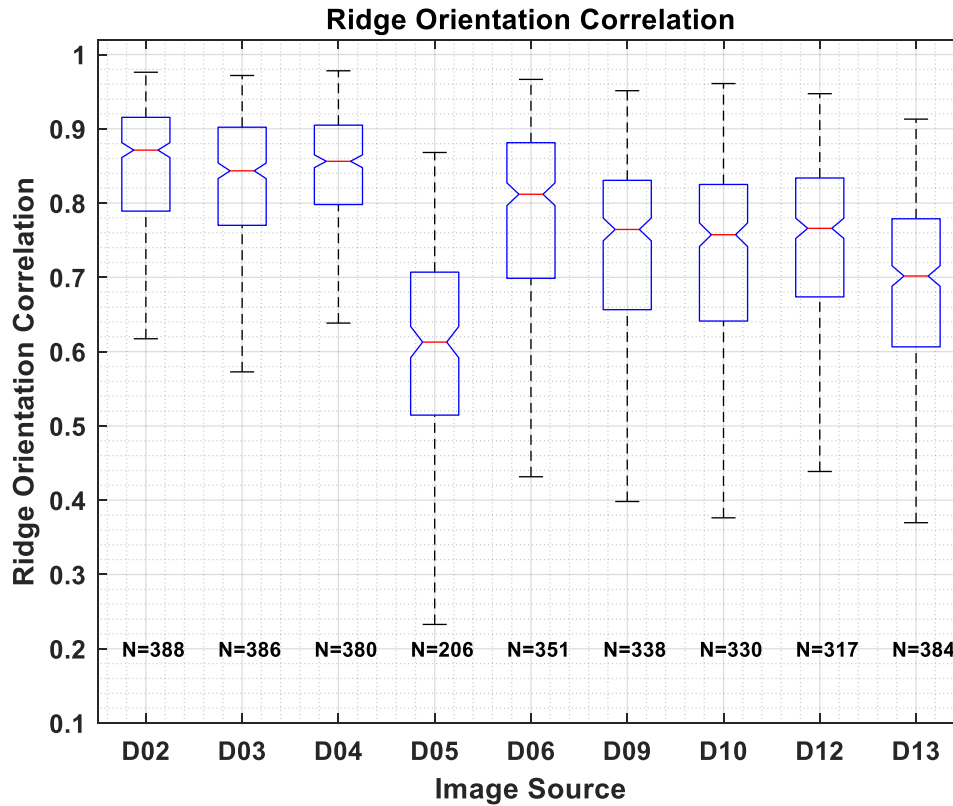


Figure 6 – Distributions of Ridge Orientation Correlation for contact devices 02, 03, and 04 compared to that of mobile contactless fingerprint capture devices.

### 3.7. Inverse RMS Difference of Spectral Image Validation Verification (SIVV) Signals

This metric examines the difference in overall power spectral content (frequency domain, as opposed to spatial domain as is the case for many of the other tests in this study) for the images being compared. Of course, in the present experimental case these are two fingerprint images collected from the same finger using the same device in very close temporal proximity. Identical

Legend:	D02 : Contact, Electroluminescent	D03 : Contact, FTIR	D04 : Contact, FTIR	D05 : Contactless, Mobile	D06 : Contactless, Mobile
	D07 : Contactless, Mobile	D09 : Contactless, Mobile	D10 : Contactless, Mobile	D12 : Contactless, Mobile	D13 : Contactless, Mobile

images should score 1.0 on this metric. In the present case we see all devices with medians in approximately the same range of the high ninety percent. Variance is similar across most devices with D05 and D12 being exceptions. This could be the result of noise in the contactless images contributing to spectral differences.

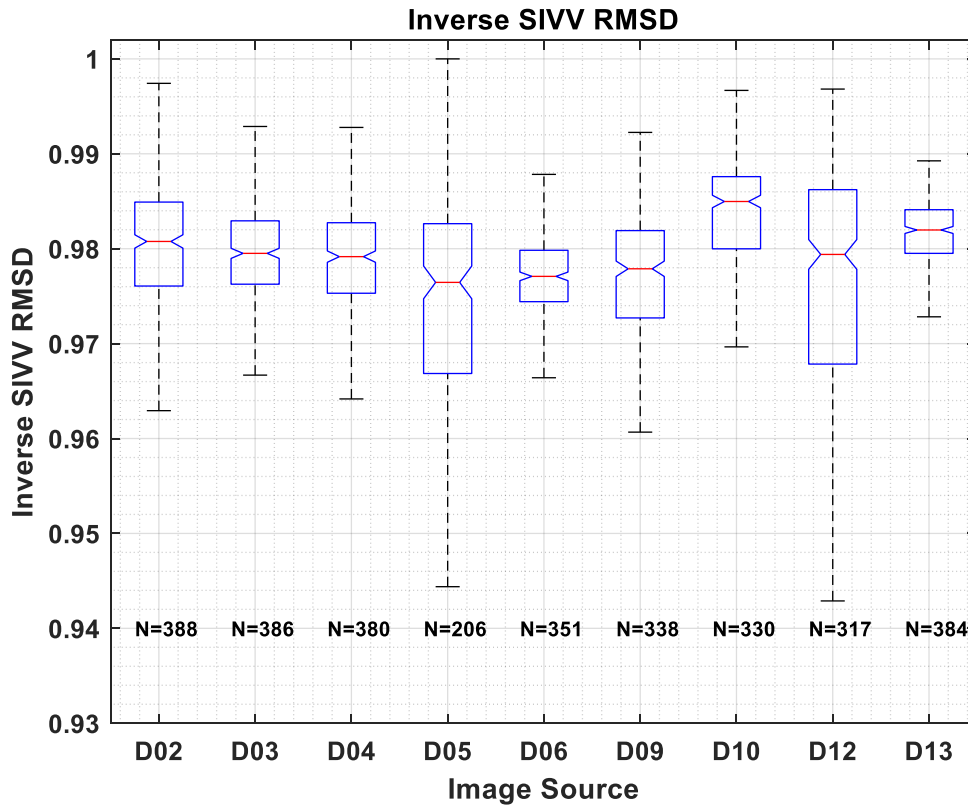


Figure 7 – Distributions of inverse RMSD off SIVV signals for contact devices 02, 03, and 04 compared to that of mobile contactless fingerprint capture devices.

### 3.8. SIVV Correlation

Rather than measuring spectral power differences across frequencies, this metric examines the parallelism of the 1D SIVV radial power spectra.

Legend:	D02 : Contact, Electroluminescent	D03 : Contact, FTIR	D04 : Contact, FTIR	D05 : Contactless, Mobile	D06 : Contactless, Mobile
	D07 : Contactless, Mobile	D09 : Contactless, Mobile	D10 : Contactless, Mobile	D12 : Contactless, Mobile	D13 : Contactless, Mobile

Examination of SIVV Correlation again shows that contact collection devices demonstrate low variance in the collected images, as well as higher SIVV correlation. This however is not universal and contactless devices D06, D10, D12 and D13 are competitive with contact collection devices.

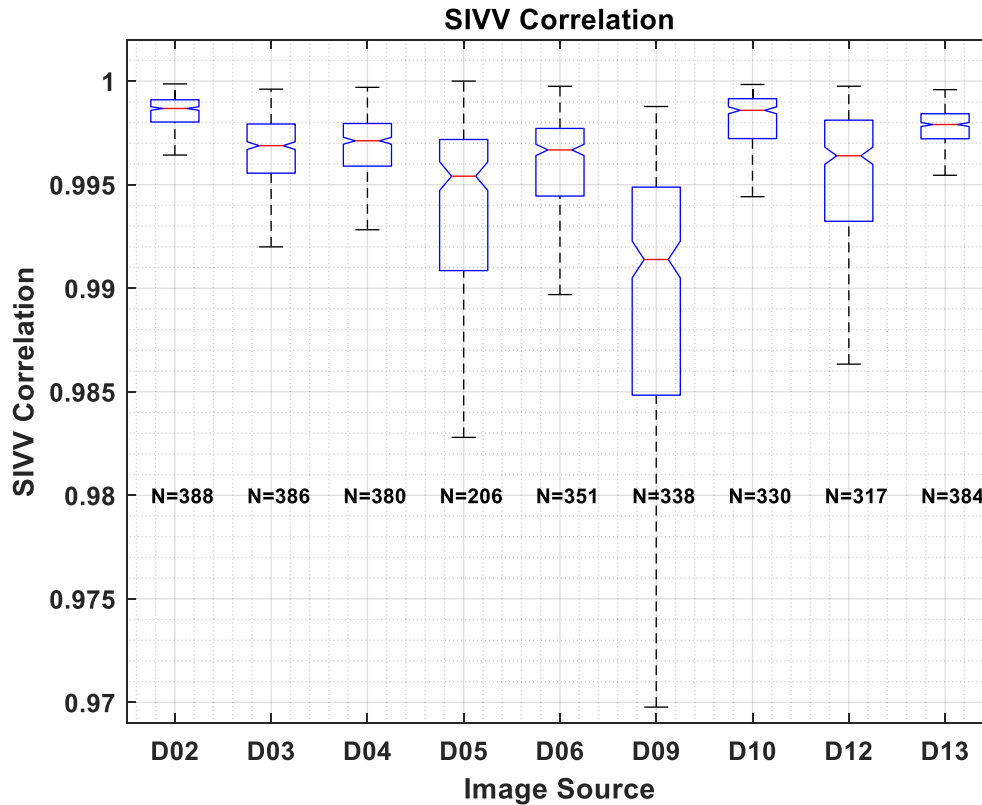


Figure 8 – Distributions of Correlation of SIVV signals for contact devices 02, 03, and 04 compared to that of mobile contactless fingerprint capture devices

#### 4. Conclusions

Contact collection requires applying mechanical pressure by the finger to a collection medium, and given the plasticity of the finger, this mechanical pressure introduces deformation to the finger relative to its original shape.

Because contactless collection devices do not require any mechanical force on the finger to conduct a collection that the deformation normally introduced to fingers during contact collection is not present in contactless collection. Accordingly, it was hypothesized that displacement of minutiae should be lower for contactless acquisition than for contact. This proved to not be the case. We have discussed various sources of distortion with contactless fingerprint acquisition in [13] and find here that these distortion factors are present even with

Legend:	D02 : Contact, Electroluminescent	D03 : Contact, FTIR	D04 : Contact, FTIR	D05 : Contactless, Mobile	D06 : Contactless, Mobile
	D07 : Contactless, Mobile	D09 : Contactless, Mobile	D10 : Contactless, Mobile	D12 : Contactless, Mobile	D13 : Contactless, Mobile

repeat capture using the same device. We note that in the present case the contact-collected images were plain impressions requiring only the downward pressure of the finger onto the device platen without the lateral stresses that might occur in collection of a rolled fingerprint impression. Were rolled fingerprints available we might have found greater minutiae displacement. We plan to evaluate this in a follow-on study.

Furthermore, it was hypothesized that repeat fingerprint collection in close temporal adjacency will yield fingerprint images that have had minimal environmental impact introduced as a result of the small delay between captures.

Therefore, it was hypothesized that images captured using contactless devices in close temporal proximity should exhibit very little deformation and offer optimal similarity given the repeat capture closely in time from the same device and by the same operator.

Results of this study, with some noted exceptions, showed that in general, contact collection devices continue to excel over the contactless collection devices in terms of similarity in repeat captures close in time. Furthermore, all experimental cases (again with some noted exceptions) showed that contact collected images represent less variability in temporally adjacent captures relative to the new contactless devices.

With this, we conclude that while contactless devices carry with them the promise of faster capture without making any contact with the subject, the images captured by these devices may have greater variability across successive captures and may not perform as well as contact-collected images in various stages of friction ridge image processing including automated matching.

Legend:	D02 : Contact, Electroluminescent	D03 : Contact, FTIR	D04 : Contact, FTIR	D05 : Contactless, Mobile	D06 : Contactless, Mobile
	D07 : Contactless, Mobile	D09 : Contactless, Mobile	D10 : Contactless, Mobile	D12 : Contactless, Mobile	D13 : Contactless, Mobile

## References

- [1] Alice V. Maceo. *Qualitative Assessment of Skin Deformation: A Pilot Study*, Journal of Forensic Identification, 390 / 59 (4), 2009.
- [2] William F. Leo, C.L.P.E. *Distortion versus Dissimilarity in Friction Skin Identification*, Journal of Forensic Identification, vol. 48 #2, pp 125 -- 129.), March/April 1998 issue.
- [3] Fagert, Michael, *Quantifying the Limits of Fingerprint Variability* (2014). Graduate Theses, Dissertations, and Problem Reports. 327. <https://researchrepository.wvu.edu/etd/327>.
- [4] Qinghai Gao and Xiaowen Zhang. *A Study of Distortion Effects on Fingerprint Matching*, Computer Science and Engineering 2012, 2(3): 37-42, DOI: 10.5923/j.computer.20120203.06.
- [5] Arun Ross, Sarat C. Dass, Anil K. Jain. *Estimating Fingerprint Deformation*, Appeared in Proc. of International Conference on Biometric Authentication (ICBA), LNCS vol. 3072, pp. 249-255, Hong Kong, July 2004.
- [6] Miss.Renuka Dhaka, Prof.S.D.Jondhale. *Review on Detection and Distortion Field Estimation from Distorted Fingerprints Images*, International Research Journal of Engineering and Technology (IRJET) e-ISSN: 2395 -0056, Volume: 02 Issue: 09, Dec-2015
- [7] Qijun Zhao, Anil Jain, Gil Abramovich. *3D to 2D Fingerprints: Unrolling and Distortion Correction*, Proceedings of the International Joint Conference on Biometrics, Washington, D.C., October 2011.
- [8] Peter Wild, Franz Daubner, Harald Penz, Gustavo Fernández Domínguez *Comparative Test of Smartphone Finger Photo vs.Touch-based Cross-sensor Fingerprint Recognition*, 2019 7th International Workshop on Biometrics and Forensics (IWBF), 1-6.
- [9] Steven A. Grosz, Joshua J. Engelsma and Anil K. Jain. *C2CL: Contact to Contactless Fingerprint Matching*, arXiv:2104.02811v3 [cs.CV], <https://doi.org/10.48550/arXiv.2104.02811>.
- [10] Parmeshwar Birajadari, Meet Haria, Pranav Kulkarni, Shubham Gupta, Pradsad Joshi, Brijesh Singh and Vikram Gadre. *Towards smartphone-based touchless fingerprint recognition*, Sādhanā (2019) 44:161, <https://doi.org/10.1007/s12046-019-1138-5>.
- [11] H, Yin, J. Hu, and J. Xu. *Contactless fingerprint enhancement via intrinsic image decomposition and guided image filtering*, 2016 IEEE 11th Conference on Industrial Electronics and Applications (ICIEA), Hefei, China, 2016, pp. 144-149, Doi: 10.1109/ICIEA.2016.7603567.
- [12] C. Kauba, D. Söllinger, S. Kirchgasser, A. Weissenfeld, G. Fernández Domínguez, B. Strobl, A. Uhl. *Towards Using Police Officers' Business Smartphones for Contactless Fingerprint Acquisition and Enabling Fingerprint Comparison against Contact-Based Datasets*. Sensors 2021, 21, 2248. <https://doi.org/10.3390/s21072248>.
- [13] J. Libert, J. Grantham, B. Bandini, S. Wood, M. Garris, K. Ko, F. Byers, C. Watson. *Guidance for Evaluating Contactless Fingerprint Acquisition Devices*, NIST Special Publication 500-305, National Institute of Standards and Technology, July 2018, <https://doi.org/10.6028/NIST.SP.500-305> .
- [14] J. Libert , J. Grantham, B. Bandini, K. Ko, S. Orandi and C. Watson. (2020), *Interoperability Assessment 2019: Contactless-to-Contact Fingerprint Capture*, NIST Interagency/Internal Report (NISTIR), National Institute of Standards and Technology,

- Gaithersburg, MD, [online], <https://doi.org/10.6028/NIST.IR.8307> (Accessed March 2, 2023)
- [15] S. Orandi, J. Libert, B. Bandini, K. Ko, J. Grantham and C. Watson (2020), *Evaluating the Operational Impact of Contactless Fingerprint Imagery on Matcher Performance*, NIST Interagency/Internal Report (NISTIR), National Institute of Standards and Technology, Gaithersburg, MD, [online], <https://doi.org/10.6028/NIST.IR.8315> (Accessed March 2, 2023)
- [16] U. I Oduah., I. F Kevin, D. O.Oluwole, J. U. Izunobi *Towards a high-precision contactless fingerprint scanner for biometric authentication*. Array (N Y). 2021 Sep;11:100083. doi: 10.1016/j.array.2021.100083. Epub 2021 Aug 6. PMID: 35083429; PMCID: PMC8343378.
- [17] Steven A. Grosz, Steven A., Engelsma, Joshua J., Liu, Eryun, Jain, Anil K. C2CL: *Contact to Contactless Fingerprint Matching*, IEEE Transactions on Information Forensics and Security Volume 172022 pp 196–210 <https://doi.org/10.1109/TIFS.2021.3134867>
- [18] B. Williams, J. McCauley, J. Dando, N. Nasrabadi and J. Dawson. *Interoperability of Contact and Contactless Fingerprints Across Multiple Fingerprint Sensors*, (2021) International Conference of the Biometrics Special Interest Group (BIOSIG), Darmstadt, Germany, 2021, pp. 1-7, doi: 10.1109/BIOSIG52210.2021.9548284.
- [19] P. Wild, F. Daubner, H. Penz and , G. F. Domínguez. *Comparative Test of Smartphone Finger Photo vs. Touch-based Cross-sensor Fingerprint Recognition*, 2019 7th International Workshop on Biometrics and Forensics (IWBF), Cancun, Mexico, 2019, pp. 1-6, doi: 10.1109/IWBF.2019.8739191.
- [20] A. M. Bazen and S. H. Gerez. *Fingerprint matching by thin-plate spline modelling of elastic deformations*, Pattern Recognition, vol. 36, no. 8, pp. 1859–1867, 2003.
- [21] R. Cappelli, D. Maio and D. Maltoni. *Modelling plastic distortion in fingerprint images*, in International Conference on Advances in Pattern Recognition. Springer, 2001, pp. 371–378.
- [22] A. Senior and R. Bolle. *Improved Fingerprint Matching by Distortion Removal*. IEICE Trans. Information and Systems 2001, 84 (7), 825-831.
- [23] A. Ross, S. Dass and A.Jain. *A deformable model for fingerprint matching*, Pattern Recognition, vol. 38, no. 1, pp. 95–103, 2005.
- [24] Mobile Fingerprinting Innovation Technology Challenge (mFIT Challenge), NIST Public Safety Communications Research Division, Boulder, CO, 2021. <https://www.nist.gov/ctl/pscr/open-innovation-prize-challenges/past-prize-challenges/2021-mobile-fingerprinting>
- [25] FBI/CJIS, “Electronic Biometric Transmission Specification (EBTS) Technical and Operational Update (TOU) 11.0”, Federal Bureau of Information Criminal Justice Information Systems, Clarksburg, WV, May 22, 2018, <https://fbibiospecs.fbi.gov/file-repository/>.
- [26] Personal Identity Verification (PIV) *Image Quality Specifications for Single Finger Capture Devices*, FBI/CJIS Biometric Specifications, 10 July 2006, <https://fbibiospecs.fbi.gov/file-repository/pivspec.pdf/view> (Retrieved 03/30/2023).
- [27] K. Ko, J. Grantham, B. Bandini and J. Libert. NIST Fingerprint Registration and Comparison Tool (NFRaCT), V1.0.0, 07/ 21/2022, <https://www.nist.gov/services-resources/software/nist-fingerprint-registration-and-comparison-tool-nfract>
- [28] J. Libert, S. Orandi, J. Grantham, B. Bandini, K. Ko, C. Safford, M. Staymates and C. Watson. *Specification for Interoperability Testing of Contactless Fingerprint Acquisition*

- Devices*, v1.0, NIST Special Publication 500-336, National Institute of Standards and Technology, June 2022. <https://doi.org/10.6028/NIST.SP.500-336>.
- [29] J. Grantham, K. Ko, B. Bandini and J. Libert. NIST Fingerprint Registration and Comparison Tool (NFRaCT), Release 1.0.0, National Institute of Standards and Technology (NIST), July 2022, <https://www.nist.gov/services-resources/software/nist-fingerprint-registration-and-comparison-tool-nfract> .
- [30] Važan, R, SourceAFIS open source fingerprint matcher, <https://sourceafis.machinezoo.com>. Retrieved 02/14/2022.
- [31] B. Bandini and J. Libert. NIST Fingerprint Registration Library (NFRL), 2022, <https://github.com/usnistgov/NFRL>
- [32] W. Zhou, A. C. Bovik, H. R. Sheikh, and E. P. Simoncelli. *Image Quality Assessment: From Error Visibility to Structural Similarity*. IEEE Transactions on Image Processing. Vol. 13, Issue 4, April 2004, pp. 600–612.
- [33] R. Thai. Fingerprint Image Enhancement and Minutiae Extraction, Student Report submitted in partial fulfillment of requirements for the Honours Programme of the School of Computer Science and Software Engineering, The University of Western Australia, 2003, <https://www.peterkovesi.com/studentprojects/raymondthai/RaymondThai.pdf> , (Retrieved 06/18/2018)
- [34] Peter Kovesi. MATLAB and Octave Functions for Computer Vision and Image Processing. Available from: <http://www.peterkovesi.com/matlabfns/>
- [35] J. Libert, J. Grantham and S. Orandi. *A 1D Spectral Image Validation/Verification Metric for Fingerprints*, NIST Interagency Report 7599, August 2009 [http://ws680.nist.gov/publication/get\\_pdf.cfm?pub\\_id=903078](http://ws680.nist.gov/publication/get_pdf.cfm?pub_id=903078), Retrieved 01/29/2021
- [36] Wikimedia Commons, Boxplot vs. PDF, [https://commons.wikimedia.org/wiki/File:Boxplot\\_vs\\_PDF.svg](https://commons.wikimedia.org/wiki/File:Boxplot_vs_PDF.svg) .(Retrieved 04/05/2023)

## Appendix A. Glossary

NFRaCT	NIST Fingerprint Registration and Comparison Tool (software)
NIST	National Institute of Standards and Technology
PIV	Personal Identity Verification
ppi	Pixels per inch (the customary unit of sampling for digital fingerprints)
ppmm	Pixels per millimeter
RMSD	Root-Mean-Squared Deviation (or Difference)
ROI	Region of Interest
SIVV	Spectral Image Validation Verification

## Appendix B. Box and Whisker Plots

In the metric analyses above we summarize the measurement results in most cases using the data visualization graphic known as the boxplot or box and whisker plot. This method enables simultaneous display of measurement distributions for multiple experimental conditions, or in the present case, devices or comparisons of measurements between devices.

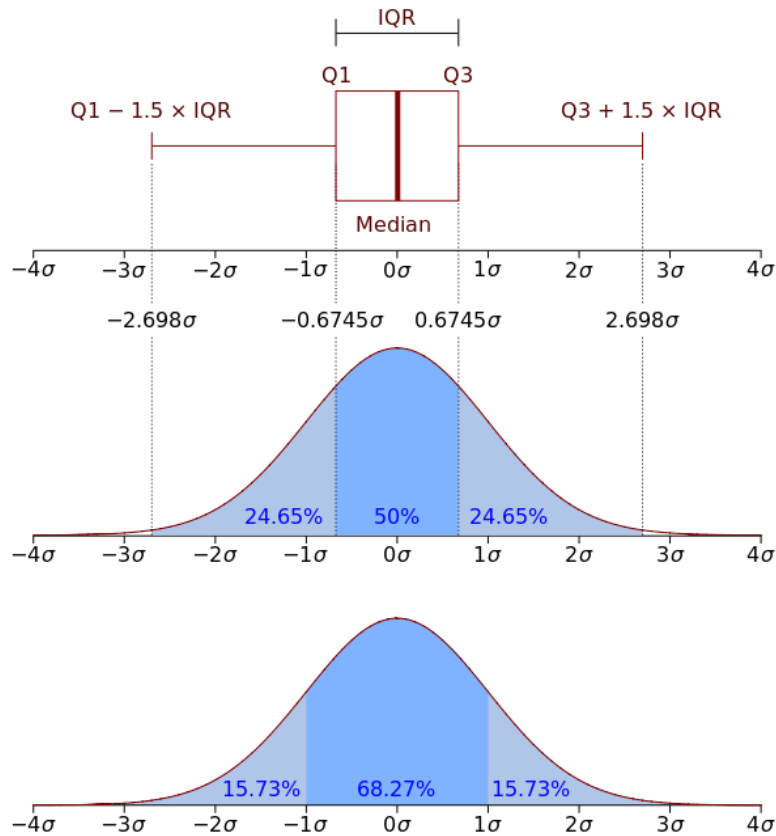


Figure 9 – Relationship between the boxplot of normally distributed data compared to the standard normal distribution for illustrative purposes. [36]

In the Figure 9 above we see that the outstanding feature of the boxplot is, of course, the box having the median marked by the central line. In the boxplots used in the present study, the median is surrounded by a notch representing the 95 % confidence interval about the median value. Interpreting the boxplot, it is significant that the box contains 50 % of the distribution and 24.65 % between the limits of the box, Q1 and Q3, and the ends of each whisker. Note that corresponding to the normal distribution, this leaves approximately 0.35 % of the distribution beyond the limits of the whiskers. In these boxplots, these values, considered outliers, are omitted from the display.